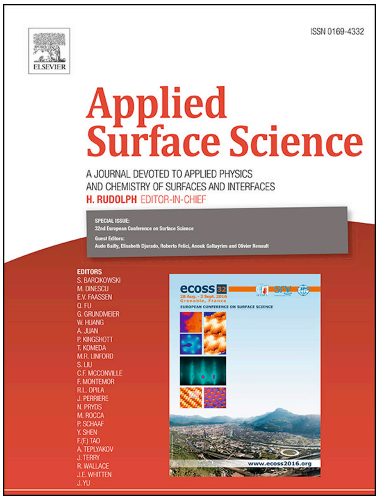

ISSN 0169-4332

Applied Surface Science

A JOURNAL DEVOTED TO APPLIED PHYSICS AND CHEMISTRY OF SURFACES AND INTERFACES

H. RUDOLPH EDITOR-IN-CHIEF

Full Length Article

Density-Functional Theory Molecular Dynamics Simulations of a-HfO_2/a-SiO_2/SiGe and a-HfO_2/a-SiO_2/Ge with a-SiO_2 and a-SiO suboxide interfacial layers

Evgueni A. Chagarov, Mahmut S. Kavrik, Ziwei Fang, Wilman Tsai, Andrew C. Kummel

PII: S0169-4332(18)30384-2
DOI: https://doi.org/10.1016/j.apsusc.2018.02.041
Reference: APSUSC 38499

To appear in: *Applied Surface Science*

Received Date: 1 September 2017
Revised Date: 26 January 2018
Accepted Date: 4 February 2018

Please cite this article as: E.A. Chagarov, M.S. Kavrik, Z. Fang, W. Tsai, A.C. Kummel, Density-Functional Theory Molecular Dynamics Simulations of a-HfO_2/a-SiO_2/SiGe and a-HfO_2/a-SiO_2/Ge with a-SiO_2 and a-SiO suboxide interfacial layers, *Applied Surface Science* (2018), doi: https://doi.org/10.1016/j.apsusc.2018.02.041

Density-Functional Theory Molecular Dynamics Simulations of a-HfO_2/a-SiO_2/SiGe and a-HfO_2/a-SiO_2/Ge with a-SiO_2 and a-SiO suboxide interfacial layers.

Evgueni A. Chagarov[1], Mahmut S. Kavrik[1], Ziwei Fang[2], Wilman Tsai[2], Andrew C. Kummel[1]

[1]Chemical and Materials Sciences, University of California, San Diego

[2] TSMC

Comprehensive Density-Functional Theory (DFT) Molecular Dynamics (MD) simulations were performed to investigate interfaces between a-HfO_2 and SiGe or Ge semiconductors with fully-stoichiometric a-SiO_2 or sub-oxide SiO interlayers. The electronic structure of the selected stacks was calculated with a HSE06 hybrid functional. Simulations were performed before and after hydrogen passivation of residual interlayer defects. For the SiGe substrate with Ge termination prior to H passivation, the stacks with a-SiO suboxide interlayer (a-HfO_2/a-SiO/SiGe) demonstrate superior electronic properties and wider band-gaps than the stacks with fully coordinated a-SiO_2 interlayers (a-HfO_2/a-SiO_2/SiGe). After H passivation, most of the a-HfO_2/a-SiO_2/SiGe defects are passivated. To investigate effect of random placement of Si and Ge atoms additional simulations with a randomized SiGe slab were performed demonstrating improvement of electronic structure. For Ge substrates, before H passivation, the stacks with SiO suboxide interlayer (a-HfO_2/a-SiO/Ge) also demonstrate wider band-gaps than the stacks with fully coordinated a-SiO_2 interlayers (a-HfO_2/a-SiO_2/Ge). However, even for a-HfO_2/a-SiO/Ge, the Fermi level is shifted close to the conduction band edge (CBM) consistent with Fermi level pinning. Again, after H passivation, most of the a-HfO_2/a-SiO_2/Ge defects are passivated. The stacks with fully coordinated a-SiO_2 interlayers have much stronger deformation and irregularity in the semiconductor (SiGe or Ge) upper layers leading to multiple under-coordinated atoms which create band-edge states and decrease the band-gap prior to H passivation.

I. Introduction.

Although Ge is less popular in semiconductor transistor applications than Si, Ge has compelling properties for scaled low power electronics. Ge is one of a few semiconductors that can provide significantly higher hole mobility than Si and, therefore, is being extensively investigated for p-channel metal-oxide-semiconductor-field-effect-transistors (MOSFET). SiGe alloys provide a compromise in terms of higher hole mobility and ease of integration onto Si wafers and facile strain engineering [1]. Enhanced transport features with p-type metal-oxide-semiconductor (PMOS) in SiGe fin field-effect transistor (FinFET) structures include very high hole mobility ($457cm^2V^{-1}s^{-1}$) for SiGe with 65-70% Ge composition [2,3].

The structural properties of amorphous oxide/semiconductor interfaces are important since they impact the electrical properties and reliability of MOSFET devices. Currently amorphous a-HfO_2 is the most widely employed high-K MOSFET gate oxide for Si channels; it is used as a substitute for traditional a-SiO_2 gate oxide to reduce gate leakage for a fixed equivalent oxide thickness. However, direct interfaces between Si and HfO_2 degrade mobility and induce threshold shifts in MOSFETs [4]. Conversely, the Si-SiO_2-HfO_2 interface uses a subnanometer SiO_2 interlayer to reduce remote phonon scattering and Si dangling bonds, thereby creating better mobility and threshold voltage [4-8]. In the present work, the effect of a-SiOx interlayer insertion between HfO_2/SiGe was investigated to obtain low interface defect density. The present DFT-MD simulations provide detailed atomistic insight into the physical processes in the a-HfO_2/a-SiOx/SiGe and a-HfO_2/a-SiOx/Ge interfaces logically complementing experimental research and providing directions for further improvement of interface processing.

II. Stack Formation and Simulation Procedure.

All DFT simulations were performed with the Vienna *ab initio* simulation package (VASP) using projector augmented-wave (PAW) pseudopotentials (PPs) and the Perdew–Burke–Ernzerhof (PBE) exchange-correlation functional [9-14]. The *a*-HfO_2 sample was stoichiometric and included 40 Hf and 80 O atoms. Several a-HfO_2 samples were generated using hybrid classical and DFT-MD simulations including annealing, cooling and relaxation. The amorphous sample quality was verified via radial-distribution function (RDF) main peak positions, average nearest neighbor numbers, nearest neighbor distributions, and DFT calculated band-gaps demonstrating good correlation to available simulated and experimental reference properties [15-20]. The sample with the best match to experimental data was selected and used for simulations. The amorphous samples were generated to match the Ge(001) surface area and used for both Ge(001) and SiGe(001) since their lattice constants differ only by 3%. A more detailed explanation of a-HfO_2 sample generation was presented elsewhere [21].

The $Si_{0.5}Ge_{0.5}$ unit cell with an ordered checkerboard placement of Si and Ge atoms and the Ge unit cell were relaxed at variable volume to obtain DFT lattice constants. The initial a-SiO/SiGe slab was built including 5 Si and 5 Ge layers (8 atoms per layer) terminated by a layer of Ge atoms. To form the a-SiOx layer, 2 additional Si layers (16 Si atoms) were placed on top of the Ge-terminated SiGe and 16 O atoms were randomly placed inside and above of these 2 upper Si layers. Ge termination of SiGe was chosen since this is the most challenging case for passivation, and Ge is known to segregate to the surface of SiGe in UHV. The three bottom layers of SiGe were permanently fixed in bulk-like positions, and the bottom surface was passivated by H atoms to simulate continuous bulk. The stack was DFT-MD annealed at 800K for 1000 fs (with 1 fs timestep), cooled to 0K for 200 fs and relaxed to the ground configuration below 0.05 eV/Å force-tolerance level. To form the a-SiO_2/SiGe slab, 16 more O atoms were placed on the previous slab and annealed, cooled, relaxed according to the same procedure. To investigate effect of Si and Ge random placement, a randomized SiGe slab was built and prepared in the same way as described above keeping Si/Ge ratio equal to 1:1. The upper surface of randomized SiGe slab has 4 Si and 4 Ge atoms. The a-SiO and a-SiO_2 layers were generated on randomized SiGe slab by DFT molecular dynamics using the same procedure.

The initial a-SiO/Ge slab was built using similar procedure. It included 10 Ge layers (8 atoms per layer) with 2 additional top Si layers (16 Si atoms) and 16 O atoms randomly placed on top and inside 2 upper Si layers. The three Ge bottom layers were permanently fixed in bulk-like positions, and the bottom surface was passivated by H atoms. The a-SiO/Ge stack was DFT-MD annealed using the same procedure as for the a-SiO/SiGe slab. To form a-SiO_2/Ge slab, 16 more O atoms were placed on the final a-SiO/Ge slab and annealed, cooled, relaxed according to the same procedure.

To simulate oxide-semiconductor stacks, the same a-HfO_2 sample was placed on a-SiO/SiGe (ordered), a-SiO_2/SiGe (ordered), a-SiO/Ge, a-SiO_2/Ge slabs to have interfacial bond lengths close to equilibrium values. The HfO_2 upper surface was terminated by H atoms to passivate significantly under-coordinated Hf atoms. All 4 stacks were DFT simulated using the same procedure. The stack simulation was started with partial initial relaxation with 50 conjugate-gradient (CG) relaxation steps. The goal of the initial relaxation is not a complete relaxation of the stack, but partial alleviation of initial internal stresses produced by oxide stacking.

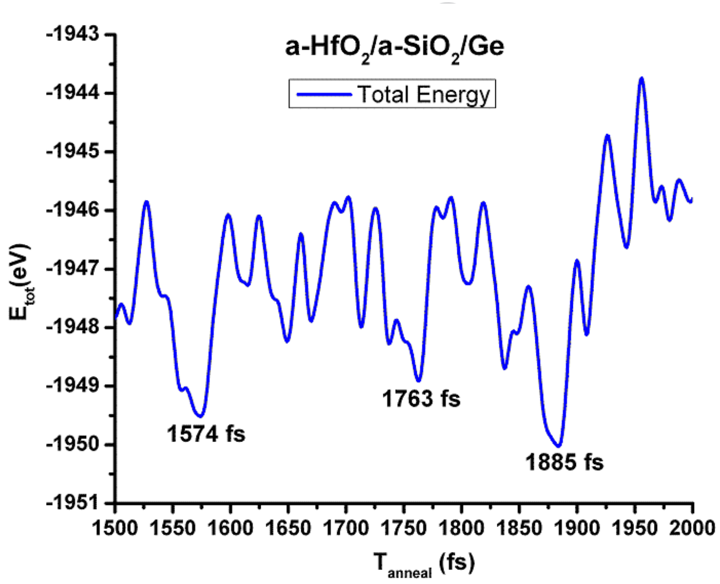

Figure 1. Total energy for an a-HfO_2/a-SiO_2/Ge stack during last 500 fs of annealing.

The stacks were DFT-MD annealed at 800K for 2000 fs with 1 fs time steps. The total energy of the stacks was plotted over time. Within the final 500 fs of annealing, 3 major energy minima were selected for every stack and corresponding system snapshots were used as starting points for subsequent cooling. This procedure produced 3 systems for every stack. Although these annealing energy minima correspond to the system in excited state at 800K, and the overall ensemble is non-adiabatic maintaining constant temperature by atom velocity rescaling every 5 timesteps; consequently, the system configurations at these energy minima are reasonable starting points for subsequent cooling and relaxation. For the a-HfO_2/a-SiO/SiGe stack, the 3 selected cooling starting points were: 1912, 1947 and 1970 fs of annealing while for the a-HfO_2/a-SiO_2/SiGe stack the 3 cooling starting points were: 1912, 1945 and 2000 fs of annealing. For the a-HfO_2/a-SiO/Ge stack, the 3 selected cooling starting points were: 1746, 1870 and 2000 fs of annealing while for the a-HfO_2/a-SiO_2/Ge stack, the 3 cooling starting points were: 1574, 1763, and 1885 fs of annealing. The total energy for a-HfO_2/a-SiO_2/Ge during annealing is presented in Fig. 1.

Starting from the 3 selected energy minima for the last 500 fs of annealing, the stacks were cooled to 0K for 200 fs and relaxed to the ground state below 0.05 eV/Å force-tolerance level. To increase computational performance, the previous simulations were performed at 2 K-points (Gamma and (0.5,0.5,0.5)). After final relaxation, the K-point sampling was increased to 3x3x1, and the stacks were re-relaxed producing very minor changes in geometry but improving electronic structure accuracy.

The total energies of the stacks after final relaxation are summarized in Table 1, and the final geometries of all 12 stacks are presented in Supplementary Materials Figs. S1-S4. It can be seen that final total energies are very close to each other for various annealing times for a given stack, with minor exception for a-HfO_2/a-SiO/Ge case which has difference around 2 eV for different annealing times. The analysis of final stack geometries indicates strong similarity for every stack type consistent with geometry convergence (Supplementary Materials Figs. S1-S4).

a-HfO_2/a-SiO/SiGe		**a-HfO_2/a-SiO/Ge**	
Time (fs)	**Energy (eV)**	**Time (fs)**	**Energy (eV)**
1912	**-1862.3146**	**1746**	**-1831.3615**
1947	**-1862.3142**	**1870**	**-1833.2799**
1970	**-1862.3202**	**2000**	**-1833.3201**
a-HfO_2/a-SiO_2/SiGe		**a-HfO_2/a-SiO_2/Ge**	
Time (fs)	**Energy (eV)**	**Time (fs)**	**Energy (eV)**
1912	**-2002.7330**	**1574**	**-1974.0834**
1945	**-2002.7185**	**1763**	**-1974.0616**
2000	**-2002.9484**	**1885**	**-1974.0804**

Table 1. Final total energy of annealed-cooled-relaxed a-HfO_2/a-SiOx/SiGe(ordered) and a-HfO_2/a-SiOx/Ge stacks for different annealing time.

After final relaxation, the total energies of all 12 stacks summarized in Table 1 were analyzed to choose the stacks with the minimal energy for every stack type. The selected stacks are presented in Figs. 2,3 and include a-HfO_2/a-SiO/SiGe (1970 fs of annealing), a-HfO_2/a-SiO_2/SiGe (2000 fs of annealing), a-HfO_2/a-SiO/Ge (2000 fs of annealing) and a-HfO_2/a-SiO_2/Ge (1574 fs of annealing). To investigate effect of Si/Ge randomization in the SiGe slab, similar simulations were performed with a randomized SiGe slab. The a-HfO_2/a-SiO/SiGe (random) and a-HfO_2/a-SiO_2/SiGe (random) stacks were partially relaxed with 50 GG steps, annealed at 800K for 2000 fs, cooled to 0K for 200 fs and relaxed to the ground state configuration below 0.05 eV/Å force-tolerance level. Final configurations for the stacks with randomized SiGe are presented in Fig. 2. The a-HfO_2/a-SiOx/SiGe(random) stacks demonstrate a bit lower total energies of -1862.94 eV for a-HfO_2/a-SiO/SiGe(random) and -2003.25 eV for a-HfO_2/a-SiO_2/SiGe(random).

III. Results and Discussion.

a) Interfacial bonding and coordination analysis.

The interfacial region of the selected a-HfO_2/a-SiO/SiGe(ordered) stack has predominantly 4-fold coordinated Si atoms with one 3- and one 5-fold coordinated Si atom which is similar to a-HfO_2/a-SiO/SiGe(random) interface with all 4-fold coordinated Si atoms except one 5-fold coordinated Si (Figs. 2-a, 4-a,c). The upper surface of SiGe(ordered) slab consists of Ge atoms. The a-SiO/SiGe(ordered) interface is formed mainly by Si-Ge bonds with almost a perfect Si/Ge interface with no oxygen penetration into SiGe; however, there is one O-Ge bond. The SiGe(random) upper surface has 4 Si atoms, 4 Ge atoms and the a-SiO/SiGe(random) interface is formed by 8 Si-Ge and 8 Si-Si bonds (Fig. 4-c). The upper interface (a-HfO_2/a-SiO) with SiGe(ordered) is formed exclusively by Hf-O and Si-O bonds with no Hf-Si bonding while the same interface with SiGe(random) has one Hf-Si bond (Figs. 2, 4-c). In the interfacial region, O assumes 2- or 3-fold coordination for both SiGe(ordered) and SiGe(random). The annealing does not create deformation of the SiGe crystalline slab (Figs. 2-a, 4-a,c).

The a-HfO_2/a-SiO_2/SiGe(ordered) and a-HfO_2/a-SiO_2/SiGe(random) stacks demonstrate a different type of bonding (Figs. 2-b, 4-b,d) than a-HfO_2/a-SiO/SiGe(ordered) and a-HfO_2/a-SiO/SiGe(random) stacks. In the a-HfO_2/a-SiO_2/SiGe(ordered) stack, the oxide interlayer Si atoms bond mainly to interlayer O atoms instead of atoms on the top surface of the SiGe substrate; the a-SiO_2 interlayer forms only 2 Si-Ge bonds in addition to 6 O-Ge interfacial bonds. The a-HfO_2/a-SiO_2/SiGe(random) stack demonstrates similar behavior with interlayer Si atoms forming bonds mainly to interlayer O atoms. This can be rationalized by the Si-O and Si-Ge bond dissociation energies. For Si-Ge diatomic molecules, the bond dissociation energy is 297 kJ/mole while for Si-O diatomic molecules, it is 799.6 kJ/mole, which is almost 2.7 times higher than for Si-Ge [22]. This type of bonding creates a very distorted upper surface in the SiGe slab with several under-coordinated Ge atoms (one 2-fold and two 3-fold coordinated) for SiGe(ordered) and one 3-fold Ge, 3-fold Si for SiGe(random) (Fig. 4-b,d). For the a-HfO_2/a-SiO_2/SiGe(ordered) stack, all interfacial Si atoms are fully 4-fold coordinated and all interfacial oxygens are 2-3 fold coordinated, while interfacial layer of a-HfO_2/a-SiO_2/SiGe(random) stack has one 3-fold coordinated Si (Fig. 4-d). The a-HfO_2/a-SiO_2 interface is formed exclusively by Hf-O bonds both for SiGe(random) and SiGe(ordered) slabs. Therefore, the defects are exclusively at the a-SiO_2/SiGe interface.

The a-HfO_2/a-SiO/Ge stack (Figs. 3-a, 4-e) has interfacial bonding similar to oxygen-deficient a-HfO_2/a-SiO/SiGe (Figs. 2-a,c, 4-a,c). For the a-HfO_2/a-SiO/Ge stack, the

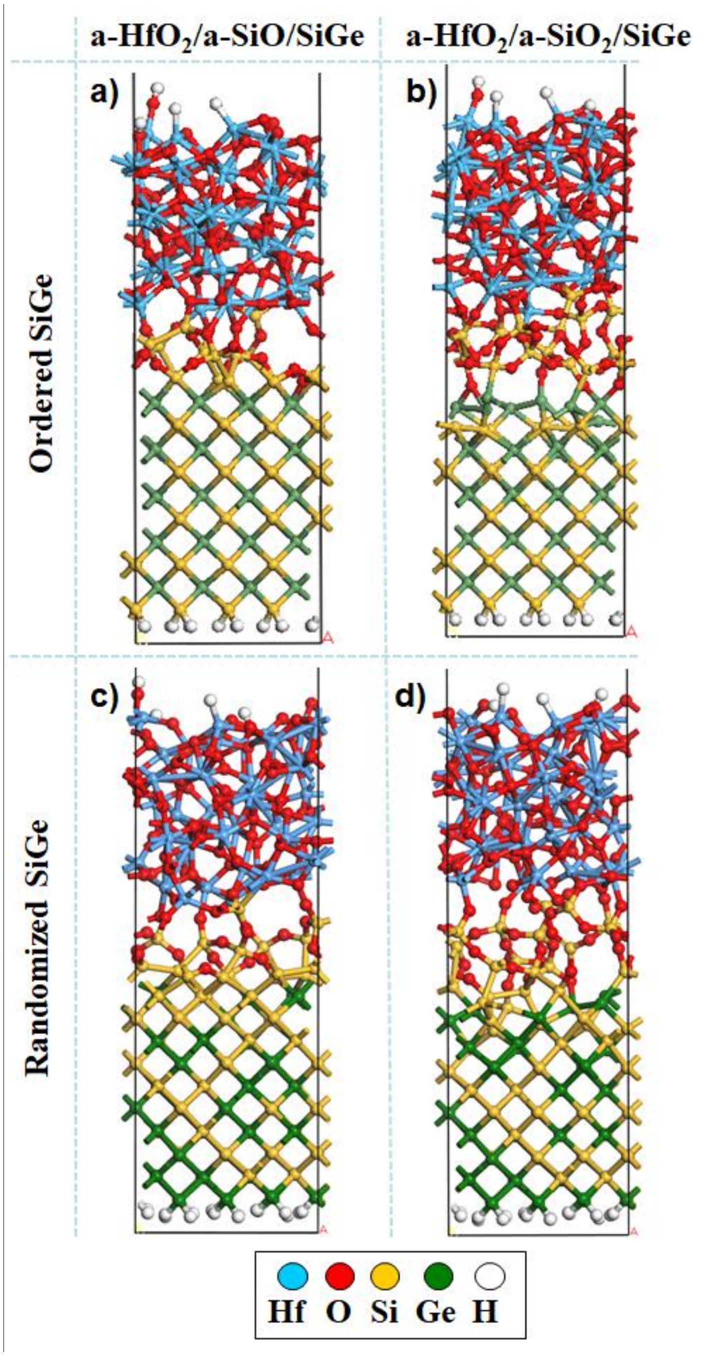

Figure 2. Final a-HfO$_2$/a-SiOx/SiGe stacks: a) a-HfO$_2$/a-SiO/SiGe(ordered), b) a-HfO$_2$/a-SiO$_2$/SiGe (ordered), c) a-HfO$_2$/a-SiO/SiGe(random), and d) a-HfO$_2$/a-SiO$_2$/SiGe(random).

interfacial a-SiO layer produces almost no deformation in interfacial Ge with all Ge 4-fold coordinated except one 3-fold coordinated Ge (Fig. 4-e). The a-SiO/Ge interface is formed exclusively by Si-Ge bonds with no O-Ge bonds. All interlayer Si atoms are 4-fold coordinated except one 3-fold and one 2-fold coordinated Si (Fig. 4-e). The ordered bonding of Si to Ge can be explained by deficiency of O atoms which forces Si atoms to bond frequently to substrate Ge trying to establish 4-fold coordination. The bonding at the a-HfO$_2$/a-SiO interface is formed predominantly by Hf-O and Si-O bonds with only 2 long and weak Hf-Si bonds (Fig. 4-e).

The a-HfO$_2$/a-SiO$_2$/Ge stack (Figs. 3-b, 4-f) demonstrates interfacial bonding similar to the corresponding a-HfO$_2$/a-SiO$_2$/SiGe (Figs. 2-b,d, 4-b,d) stack. The a-HfO$_2$/a-SiO$_2$/Ge stack shows similar enhanced Ge substrate deformation and more frequent Ge deviation from standard 4-fold coordination with one 2-fold coordinated Ge and two 3-fold coordinated Ge (Fig. 4-f). Contrary to the oxygen-deficient a-HfO_2/a-SiO/Ge stack, the lower a-SiO_2/Ge interface is formed both by Si-Ge and O-Ge bonds. All interfacial Si atoms are 4-fold coordinated. The upper HfO_2/a-SiO_2 interface is formed by Hf-O and Si-O bonds without Hf-Si bonds. Therefore, the defects are exclusively at the a-SiO_2/Ge interface.

The analysis of Figs. 2-4 demonstrates the common feature that oxygen-deficient a-SiO interlayers creates more compact interfaces with much less deformation of the substrates (SiGe or Ge) and fewer under-coordinated two-fold coordinated Ge atoms; these are the most problematic defects since it is unlikely they can be passivated with hydrogen. Conversely, fully-stoichiometric a-SiO_2 interlayers create an interface with much more significant substrate deformation and larger number of two-fold coordinated Ge atoms.

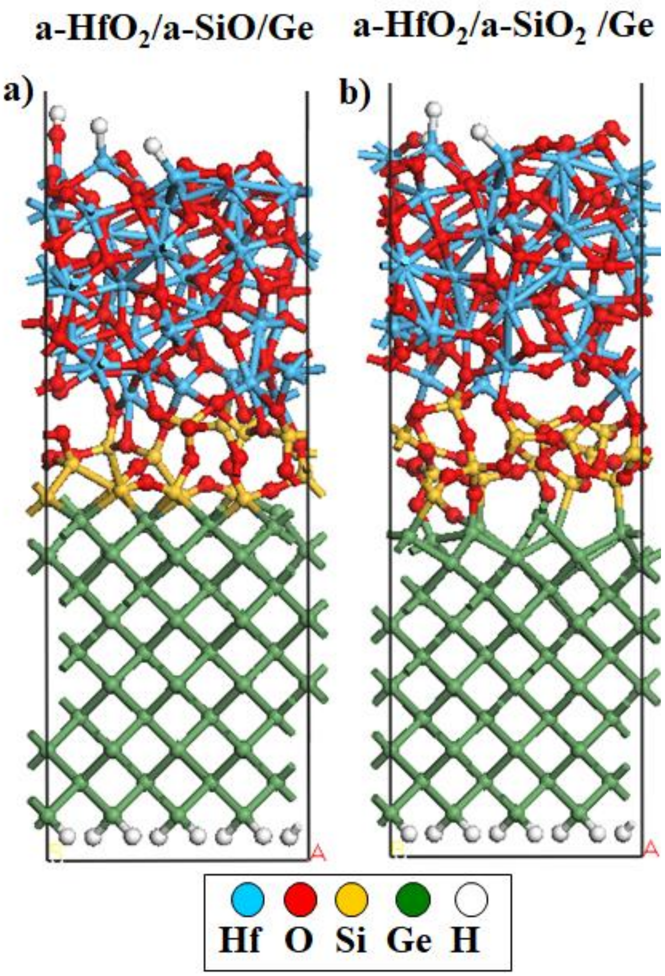

Figure 3. Final a-HfO_2/a-SiOx/Ge stacks: a) a-HfO_2/a-SiO/Ge, b) a-HfO_2/a-SiO_2/Ge.

b) Electronic structure analysis.

Since standard DFT functionals underestimate semiconductor bandgaps, which can lead to Ge bandgap disappearance, the electronic structure calculations were performed using the hybrid functional HSE06 [23,24].

Since SiGe and Ge lattice constants are slightly different for PBE *vs.* HSE06 functionals (by 1.1% for SiGe and 1.6% for Ge), the stacks were rescaled from PBE to HSE06 lattice constants and DOS curves were calculated at 3x3x1 Gamma-centered K-point grid using HSE06 functional (Fig. 5). The residual atomic forces were verified to be less than 0.05-0.08 (eV/Å). The very high computational cost of HSE06 hybrid-functional calculations makes it problematic to perform full-scale relaxation of ~270 atom system with the HSE06 force-field.

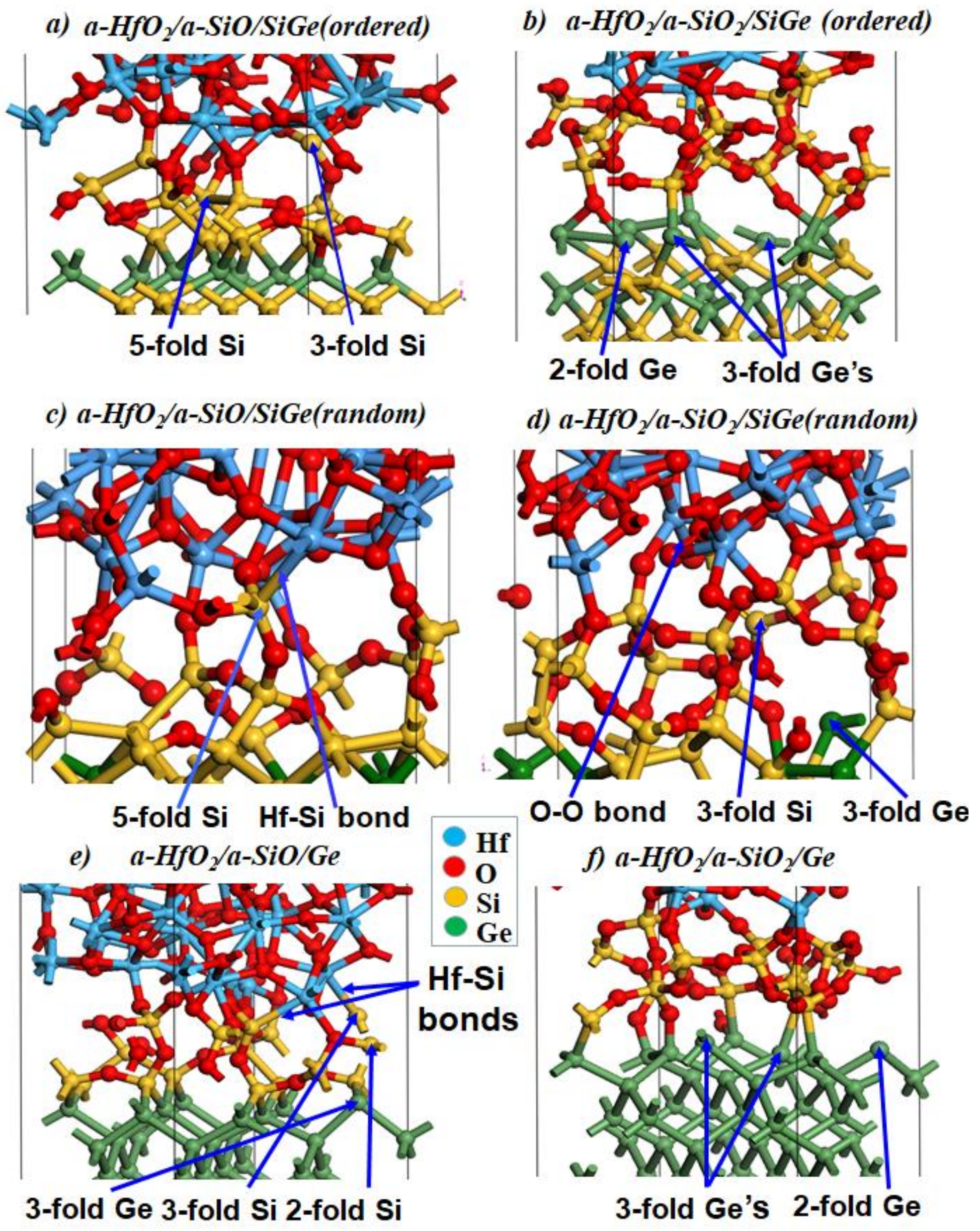

Figure 4. Final interface regions and atoms with coordination deviations. Note the fully-stoichiometric a-SiO_2 interlayer creates interfaces with much more significant substrate deformation and larger number of two-fold coordinated Ge atoms.

The DOS curves presented in Fig. 5 compare stacks with a-SiO *vs.* a-SiO_2 *vs.* corresponding bulk semiconductors. The band-gap values were estimated using eigenstates. The DOS curves presented in Fig. 5 utilize Gaussian DOS smearing to smooth the curves which somewhat decreases visual band-gap. The analysis of DOS curves clearly demonstrates that the a-HfO_2/a-SiO/SiGe(ordered) and a-HfO_2/a-

SiO/SiGe(random) stacks have close defect-free bandgaps of 1.1 eV and 1.2 eV respectively similar to the SiGe DFT-calculated bulk bandgap (1.1 eV), while the a-HfO_2/a-SiO_2/SiGe(ordered) and a-HfO_2/a-SiO_2/SiGe(random) stacks with an a-SiO_2 interlayer have significant band edge states substantially decreasing the bandgaps to 0.34 eV and 0.57 eV respectively (Fig. 5-a). For both a-SiOx interlayers, stacks with a random SiGe slab demonstrate slightly less band-edge states and a wider bandgap than with an ordered SiGe slab. This can be explained by the ordered SiGe slab having Ge-termination on SiGe upper interfaces, and Ge having a greater propensity to form midgap states than Si, while the random SiGe slab has 4 Ge and 4 Si atoms on upper interface. For all the a-SiOx interfaces on ordered and random SiGe slabs, the Fermi level was midgap.

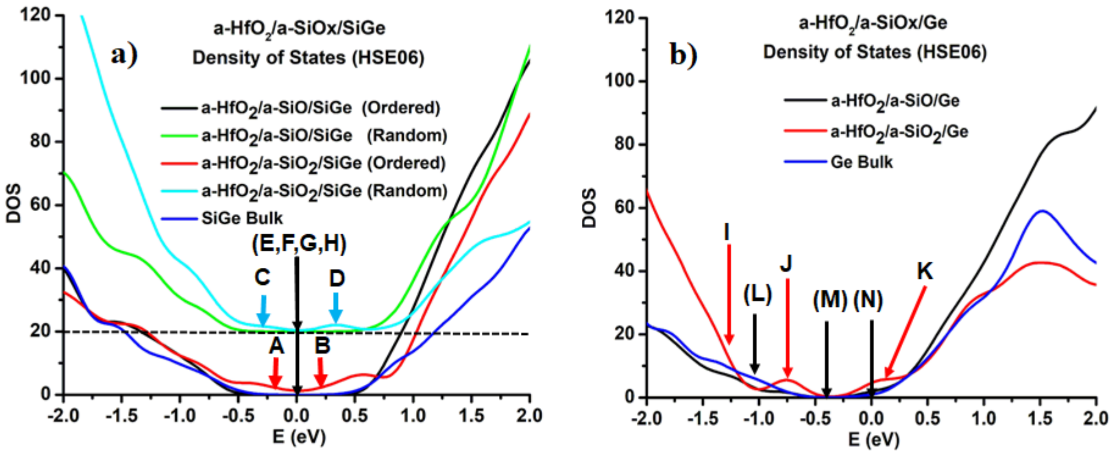

Figure 5. HSE06 DOS curves a) a-HfO_2/a-SiO/SiGe *vs.* a-HfO_2/a-SiO_2/SiGe *vs.* SiGe bulk. Arrows (A) and (B) - band-edge states for a-HfO_2/a-SiO_2/SiGe(ordered). Arrows (C) and (D) – band-edge states for a-HfO_2/a-SiO_2/SiGe(random). E_f =0.0 for all a-HfO_2/a-SiOx/SiGe stacks and for SiGe bulk (arrows (E, F, G, and H)). Curves for SiGe(random) were shifted by 20 units up to visually differentiate from the other curves. **b) a-HfO_2/a-SiO/Ge *vs.* a-HfO_2/a-SiO_2/Ge *vs.* Ge.** E_f =0.0 eV for a-HfO_2/a-SiO/Ge (arrow (N)). E_f = -1.1 eV for a-HfO_2/a-SiO_2/Ge (arrow (L)). E_f = -0.4 eV for Ge bulk (arrow (M)). States I, J, and K were examined by band-decomposed charge density analysis.

For the Ge substrate, the sub-oxide stack a-HfO_2/a-SiO/Ge has a band-gap of 0.68 eV, which is only slightly less than the Ge DFT-calculated bulk bandgap of 0.7 eV. However, its Fermi level is shifted practically to the CBM, which effectively pins the whole stack (Fig. 5-b, arrow (N)). The stack with fully-stoichiometric oxide a-HfO_2/a-SiO_2/Ge exhibits very pronounced band edge states, which significantly decrease the band gap and shift Fermi-level closer to valence band (Fig. 5-b, arrow (L)).

The HSE06 DOS curves for different annealing times are summarized in Supplementary Materials Figs. S1-S8 with their corresponding semiconductor bulk DOS. These compilations demonstrate strong convergence of DOS curves especially near the Fermi level and the same Fermi level shift for particular stack type.

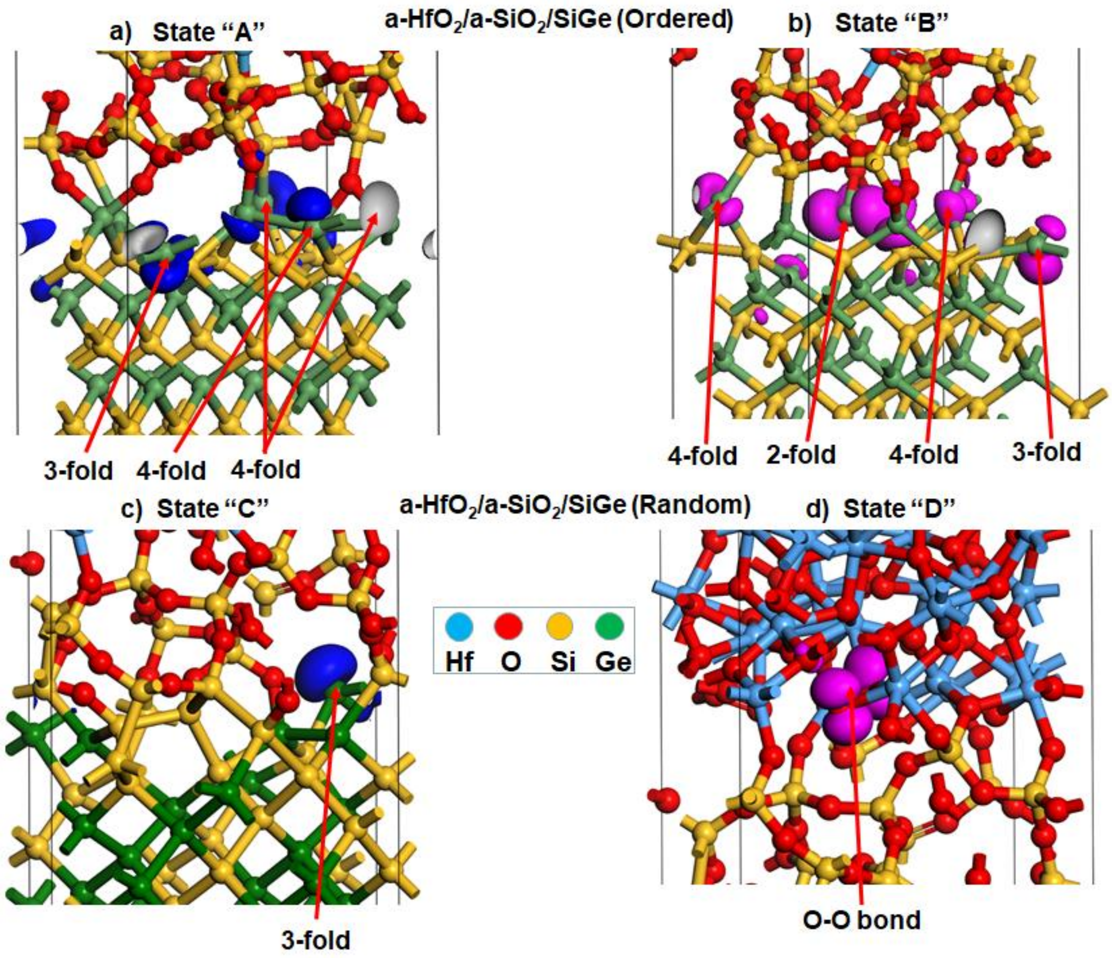

Figure 6. HSE06 band-decomposed charge density for: a,b) a-HfO_2/a-SiO_2/SiGe (ordered) valence and conduction band-edge states "A" and "B"; c,d) a-HfO_2/a-SiO_2/SiGe (random) valence and conduction band-edge states "C" and "D" (Fig. 5-a).

In addition to DOS, Bader atomic charges with core correction were calculated to investigate atom bond filling [25, 26]. As shown in Fig 5-a, a-HfO_2/a-SiO/SiGe stacks with ordered and random SiGe have a defect-free DOS without bandgap reduction. Fig. 4-a indicates that the a-HfO_2/a-SiO/SiGe(ordered) stack with a good electric structure has two atoms with abnormal coordination: 3- and 5-fold coordinated Si. According to the Bader charges, the 3-fold coordinated Si has 1.6 |e| electron loss *vs.* bulk Si atoms while the 5-fold coordinated Si has 1.3 |e| electron loss *vs.* bulk Si. The a-HfO_2/a-SiO/SiGe(random) stack has 5-fold coordinated interfacial Si with 1.8 |e| loss *vs.* bulk-Si. Therefore, large electron loss makes their bonding mainly ionic with no dangling bonds and therefore with no electronic structure perturbation.

To investigate source of band-edge states presented in Fig. 5, HSE06 band-decomposed charge density was calculated and visualized for states “A” (E=[-0.5; 0.0] eV), “B” (E=[0.0; +0.7] eV) for a-HfO_2/a-SiO_2/SiGe(ordered) and states “C” (E=[-0.5; 0.0] eV), “D” (E=[0.0; +0.5] eV) for a-HfO_2/a-SiO_2/SiGe(random) relative to Fermi level at 0.0 eV (Figs. 5-a, 6). The charge density clearly indicates that band-edge states “A” and “B” are localized mainly at Ge atoms at the upper surface of SiGe in contact with a-SiO_2. These band-edge states are result of significant deformation in upper layers of the SiGe slab leading to under-coordinated Ge atoms. The VBM band-edge state “A” is mainly caused by one 3-fold and two 4-fold coordinated Ge atoms. The 3-fold coordinated Ge has an electron depletion of 0.35 |e| (*vs.* bulk Ge atoms) with a partially-filled dangling bond; the first 4-fold Ge is electron depleted by 0.1 |e| with half-filled dangling bond, and the second 4-fold Ge is electron depleted by 0.2 |e| with partially-filled dangling bond. CBM band-edge state “B” is caused mainly by one 2-fold, one 3-fold, and two 4-fold coordinated Ge’s (Fig. 6). The 3-fold coordinated Ge is the same as for the state “A” with an electron depletion of 0.35 |e| and a partially-filled dangling bond while the 2-fold coordinated Ge has an electron depletion of 0.9 |e| *vs.* bulk Ge atoms and partially ionic bonding. One of 4- fold Ge’s is the same as for the state “A” with 0.2 |e| electron depletion and partially-filled dangling bond while the other has 0.8 |e| electron depletion and partially ionic bonding.

For the a-HfO_2/a-SiO_2/SiGe(random) stack, the state “C” is localized at 3-fold coordinated Ge with 0.16 |e| electron depletion *vs.* bulk Ge atoms with a half-filled dangling bond (Fig. 6-c). The state “D” is localized at a O-O bond at the a-HfO_2/a-SiO_2 interface with O’s having 0.7 |e| electron depletion *vs.* a-HfO_2 bulk O atoms (Fig. 6-d).

While the a-HfO_2/a-SiO/SiGe(ordered) and a-HfO_2/a-SiO/SiGe(random) stacks demonstrates almost defect-free DOS, the a-HfO_2/a-SiO_2/SiGe(ordered) and a-HfO_2/a-SiO_2/SiGe(random) stacks have VBM and CBM band-edge states significantly reducing the band-gap. This difference can be explained by data presented on Figs. 2-6. In case of the oxygen-deficient a-SiO interlayer, Si has a high propensity to form bonds to SiGe slab atoms resulting in almost perfect SiGe upper surface with very low distortion and low deviation from the usual 4-fold coordination. However, in case of the fully stoichiometric a-SiO_2 interlayer, Si is more driven to form Si-O bonds, which are around 2.7 times stronger than Si-Ge bonds. Oxygen creates Si-O-Ge bridges inducing significant deformation in SiGe upper layers leading to a high number of under-coordinated atoms, injecting states to the band-gap and reducing the band-gap value.

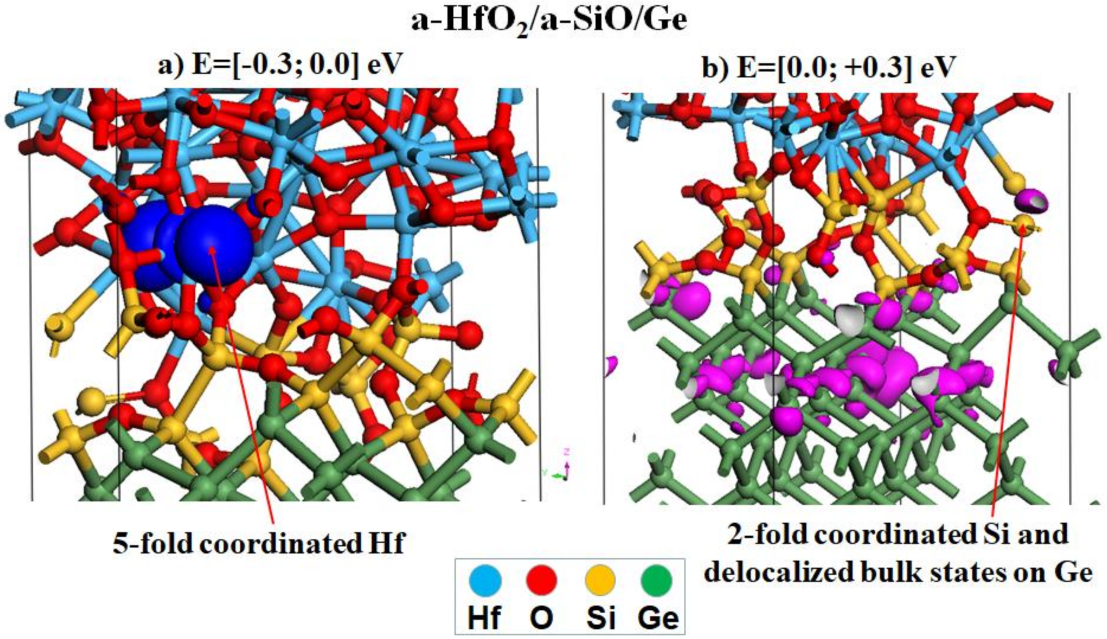

Figure 7. HSE06 band-decomposed charge density of a-HfO_2/a-SiO/Ge

a) E=[-0.3;0.0] eV vs. E_F=0 eV and b) E=[0.0;+0.3] eV *vs.* E_F=0 eV of a-HfO_2/a-SiO/Ge. (Fig. 3-a, 4-e, 5-b).

Although the a-HfO_2/a-SiO/Ge stack shows very little bandgap reduction, its Fermi level is shifted practically to CBM effectively pinning the whole stack (Fig. 5-b, arrow (N)). To investigate the states close to Fermi-level, the band-decomposed charge density was calculated for [-0.3; 0.0] and [0.0; +0.3] eV relative to E_F=0 eV and summarized in Fig. 7. The state at [-0.3; 0.0] eV is produced by a 5-fold coordinated Hf with almost planar bonding creating bond tension while the state at [0.0; +0.3] eV is produced by 2-fold coordinated Si and delocalized bulk Ge states (Fig. 7). The 2-fold coordinated Si has electron depletion of 1.4 |e| and demonstrates mainly ionic bonding with no dangling bond. Conversely, the 5-fold coordinated Hf has excessive electron charge of 0.4 |e| *vs.* bulk. It is hypothesized that the distorted Hf bonding occurs more readily on Ge than on SiGe because the SiO interlayer bonds more strongly to SiGe producing a more conformal flat layer. In case of the random SiGe slab, due to higher surface Si content, it creates a more conformal flat interfacial layer with a slightly improved electronic structure which was confirmed by electronic structure analysis presented in Fig. 5.

To investigate source of band-edge states for a-HfO_2/a-SiO_2/Ge stack band-decomposed charge-density was calculated with the HSE06 functional and visualized for states “I” (E=[-0.3; 0.0] eV), “J” (E=[0.0; +0.7] eV) and “K” (E=[-0.7; +1.3] eV) relative to E_F= -1.1 eV (arrow (L)) (Figs. 5-b,8). Similar to the SiGe system, the states “I”, “J” and “K” are localized at the upper layers of Ge substrate. The state “I” is localized at 3-fold coordinated Ge atom, which has negligible 0.01 |e| electron gain *vs.* bulk Ge indicating a half-filled dangling bond. The state “J” is localized at two 3-fold coordinated Ge atoms. One of them has minor 0.02 |e| electron gain *vs.* bulk values indicating a half-filled dangling bond, and the other Ge was mentioned previously as a source for the state “I” with 0.01 |e| electron gain and has a half-filled dangling bond. The state “K” is localized at a 2-fold coordinated Ge with 0.4 |e| electron loss and partially filled dangling bond (Fig. 8). Comparison with the a-HfO_2/a-SiO/Ge case reveals a similar trend in interfacial bonding. For an oxygen-deficient SiO interlayer, Si atoms prefer to form bonds to Ge to restore normal 4-fold coordination. This creates a Ge upper surface with majority of Ge’s having normal 4-fold coordination, very few dangling bonds, and forms a band-gap with limited reduction but Fermi level shift practically to CBM (Figs. 3-5). Conversely, in case of a fully-stoichiometric a-SiO_2 interlayer, Si-O-Ge bridges are formed leading to significant deformation in the Ge upper layers. The deformation induces formation of under-coordinated Ge atom dangling bonds injecting band-edge states and significantly decreasing the band-gap value (Figs. 3-5,7). This mechanism is very similar to the case of a-HfO_2/a-SiOx/SiGe.

Comparative analysis of all stacks indicates that undercoordinated Ge atoms produce states in the bandgap much more often than undercoordinated Si atoms. This trend can be explained by differences in bandgaps. The experimental bandgaps of Si and Ge are 1.1 eV and 0.7 eV respectively. Since the VBM and CBM of Ge are closer to midgap, they can more readily inject states into the bandgaps of SiGe or Ge. The CBM and VBM of Si are more remote from the midgap and therefore may inject states outside the SiGe or Ge bandgap. These simple metrics are consistent with the stacks having an ordered SiGe slab with a Ge-terminated upper surface possessing smaller bandgaps than the stacks having a randomized SiGe slab with 50% Si and 50% Ge upper surface (Fig. 5). The Ge substrate also has significant differences in electronic structure *vs.* the SiGe substrate. The stacks

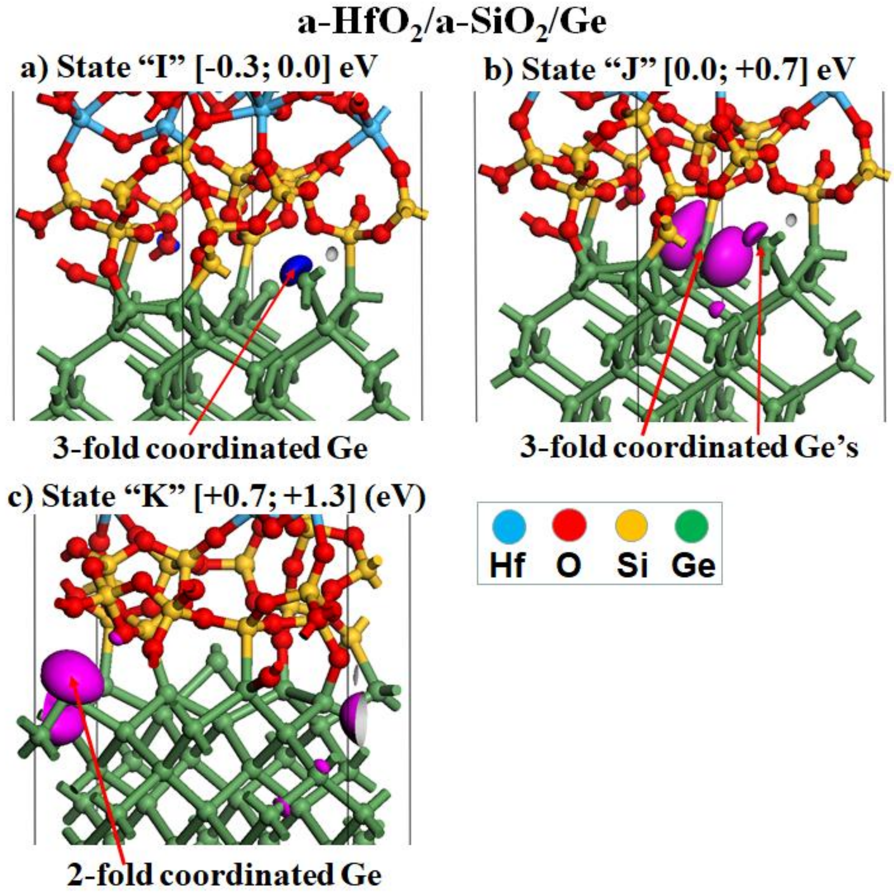

Figure 8. **HSE06 band-decomposed charge density of a-HfO_2/a-SiO_2/Ge** a) state "I" at [E_F-0.3;E_F] eV, b) state "J" at [E_F;E_F+0.7] eV and c) state "K" at [E_F+0.7;E_F+1.3] of a-HfO_2/a-SiO_2/Ge (Fig. 4-f, 5-b). E_F= -1.1 eV.

on ordered and randomized SiGe both with suboxide SiO and fully-stoichiometric SiO_2 demonstrate no significant Fermi level shift for all stacks (Fig. 5-a, Supplementary Materials Figs. S5, S6). Conversely, the stacks with Ge substrate demonstrate much larger Fermi level shifts from almost the CBM (Fig. 5-b, Supplementary Materials Fig. S7) to the VBM (Fig. 5-b, Supplementary Materials Fig. S8).

In these DFT simulations, the Fermi level is determined as a hypothetical energy level with a probability of electron filling of 0.5 (50%) at equilibrium. Therefore, if the DOS of the conduction band is much higher in amplitude than the DOS of the valence band, the Fermi level will be positioned closer to conduction band and *vice versa*. As shown in Fig. 5-b, the DOS curve for a-HfO_2/a-SiO/Ge has an elevated DOS in the conduction band relative to both the oxide stack valence band and Ge bulk conduction band. This naturally pulls Fermi level of the stack close to the CBM (Fig. 5-b, arrow "N"). Conversely, the DOS curve for the a-HfO_2/a-SiO_2/Ge has much higher DOS amplitude in the valence band region relative to the stack conduction band and Ge bulk valence band, and it naturally pulls Fermi level deep into the valence band (Fig. 5-b, arrow "L"). Contrary to such variations, all DOS curves of a-HfO_2/a-SiO_x/SiGe stacks and SiGe bulk demonstrate a much more even ratio of conduction and valence band amplitudes and less variation between curves (Fig. 5-a). This leads to much greater stability of the Fermi level for a-HfO_2/a-SiO_x/SiGe stacks.

While the Fermi level position is affected by the DOS curve shape, the DOS curve in turn is affected by chemical composition of the simulated system. Considering the Fermi level instability for a-HfO_2/a-SiO_x/Ge stacks, scaling to realistic devices and analysis of total chemical composition change can be informative. Due to high computational cost of DFT-MD simulations especially with hybrid functionals, the typical size of DFT-simulated system is usually limited to several hundred atoms. In case of realistic devices, the thickness of Ge substrate will increase significantly while interface atoms will not change very much and oxide thickness increase will be less than increase of Ge substrate thickness. As a result, contribution of Ge atoms to the total DOS curve will be more significant and the Fermi level of the stack will gravitate closer to the Fermi level position in Ge bulk (arrow "M", Fig. 5-b) probably reducing Fermi-level volatility.

c) H Passivation of Interfacial Defects.

Relaxed interfaces presented in Fig. 4 demonstrate some under-coordinated Ge and

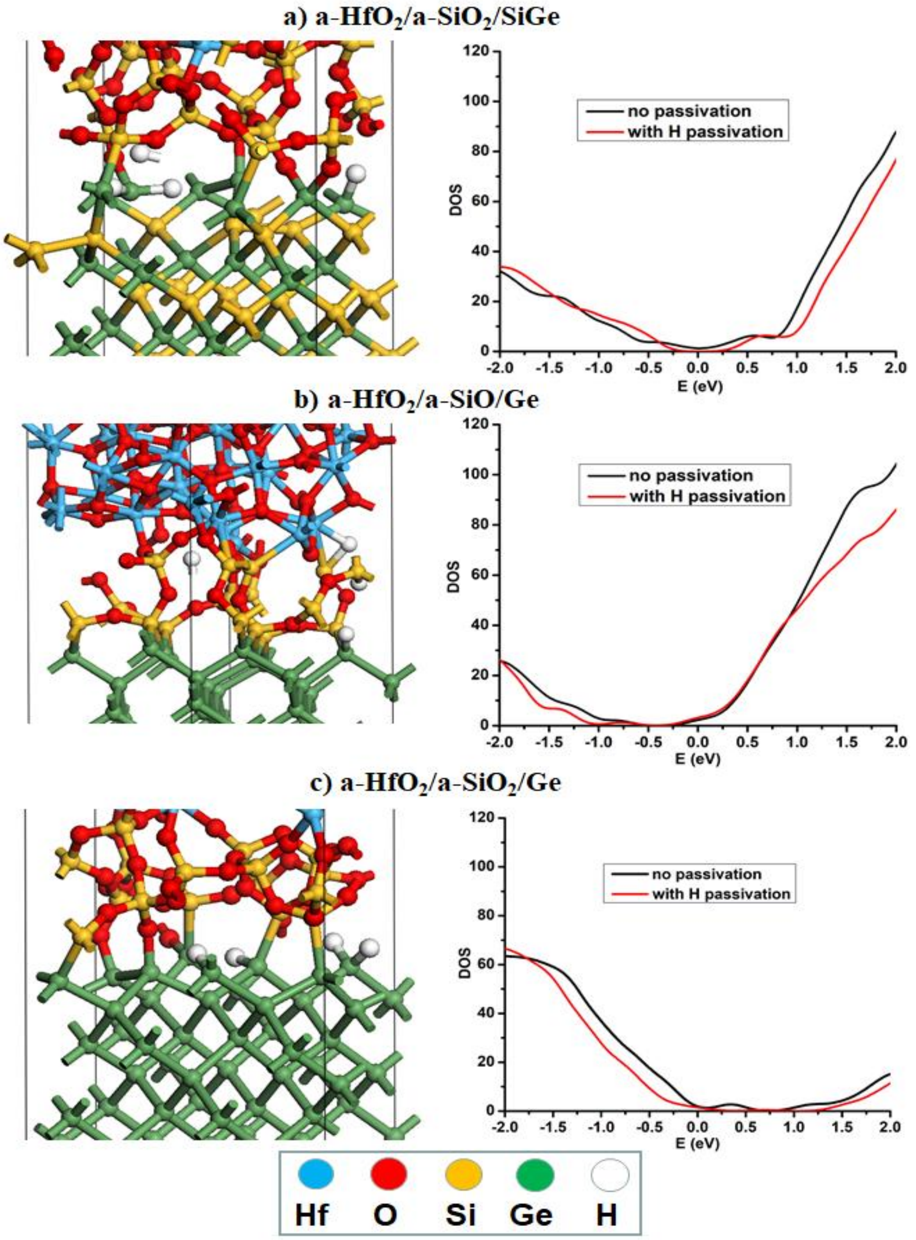

Figure 9. Relaxed stacks with interface H passivation. HSE06 DOS curves with and without H passivation**.** For all curves E_F=0 eV.

Si atoms having negative impact on the electronic structure in Figs. 5-8. These under-coordinated atoms were passivated by H atoms to restore complete 4-fold coordination and relaxed to the ground state configuration as described previously. For the a-HfO_2/a-SiO_2/SiGe(ordered) stack, one 2-fold Ge was passivated by two H's, and two 3-fold coordinated Ge's were passivated by one H each (Fig. 4-b). For the a-HfO_2/a-SiO/Ge stack, one 2-fold coordinated Si was passivated by two H atoms, one 3-fold Si was passivated by one H, and one 3-fold Ge was passivated by one H (Fig. 4-e). For the a-HfO_2/a-SiO_2/Ge stack, one 2-fold coordinated Ge was passivated by two H atoms, and two 3-fold Ge atoms were passivated by one H atom each (Fig. 4-f). After relaxation, the stacks were rescaled from PBE to HSE06 semiconductor lattice constants and HSE06 DOS curves were calculated. The final relaxed configurations together with the DOS curves are presented in Fig. 9.

The H passivation of the a-HfO_2/a-SiO_2/SiGe(ordered) stack significantly suppresses states “A” and “B” shown at Fig. 5-a and increases the bandgap from 0.34 eV to 0.96 eV which is close to a-HfO_2/a-SiO/SiGe(ordered) stack and SiGe bulk DFT bandgaps of 1.1 eV (Fig. 9-a). For the a-HfO_2/a-SiO/Ge stack, H passivation practically does not change the bandgap and the DOS shape in the bandgap region. This can be explained by the fact that both states at [-1.0; -0.5] and [-0.3; 0.0] eV of H-passivated DOS curve are localized at 5-fold coordinated Hf atom unaffected by passivation (Figs. 7-a, 9-b). The H passivation of a-HfO_2/a-SiO_2/Ge stack removes band edge states “J” and “K” shown at Fig. 5-b and significantly improves the band gap (Fig. 9-c).

IV. Comparison to Experimental Measurements.

SiGe surface oxidation has been experimentally studied by many groups. Dry (O_2) thermal oxidation, wet (steam) oxidation have been investigated and SiO_2 layer formation on the SiGe surface by thermal O_2(g) or H_2O(g) oxidation have been reported [27- 29]. Ge atoms are rejected during the oxidation process, accumulate at the SiGe - oxide interface, and cause high interface trap density. The ratio of Ge atoms in SiGe was found to be critical for Ge-rich layer formation; for substrates with less than 50% Ge, Ge piles up at the SiGe surface; conversely, for substrates with more than 50% Ge, GeOx forms at the vacuum-oxide interface as well as accumulates at oxide-SiGe interface [30, 31]. The realism of SiO and SiO_2 passivation interfaces was verified by the studies below showing that for low Ge content SiGe, a nearly pure SiO/SiO_2 interface can be formed by annealing.

Kaufman-Osborn *et al.* employed H_2O_2(g) to functionalize and passivate the $Si_{0.6}Ge_{0.4}$(001). Oxide-free SiGe(001) surfaces have Ge dimers resulting in GeOx formation after H_2O_2(g) dosing. Annealing above ~150°C induces Si exchange with surface Ge atoms to form thermodynamically favorable SiOx terminated SiGe(001). For Al_2O_3/SiGe, trimethyl aluminum (TMA) ($Al(CH_3)_3$) as a reductant along with hydrogen peroxide (H_2O_2(g)) was used as an oxidant to grow Al_2O_3. No interfacial SiO_2 or GeO_2 was observed in XPS studies; XPS measurements before and after FGA are consistent with Ge-O-Al bonding before forming gas annealing and Si-O-Al after FGA [32]. The change in bonding configuration with annealing is consistent with the higher bonding enthalpy of Si-O *vs.* Ge-O bonds. These data confirm that use of a Si-O terminated SiGe is realistic for DFT modeling. Park *et al* observed similar thermodynamic effects in their XPS study of the effect of 800ºC rapid thermal annealing (RTA) on HfO_2/SiGe with 10-30% Ge [33]. The RTA decreased the thickness of the $SiGeO_x$ IL and increased the Si content of the IL. Cho *et al.* studied the interlayer between HfO_2 and $Si_{0.7}Ge_{0.3}$ [34]. After post deposition 800ºC N_2 annealing, XPS measurements showed the GeOx in the interlayer decreased while the SiOx in the interlayer increased; this composition change was associated with a decrease in trap states in CV measurements. This reaffirms that the DFT model of SiOx passivation of SiGeOx is reasonable.

Jaeger *et al*. grew a thin layer of Si on Ge to passivate the interface prior to HfO_2 ALD [35]. The quality of the interfaces was quantified with C-V measurements as a function of Si film thickness. The optimal Si passivation thickness was 4 monolayers. After ALD, the Si layer was converted to SiOx. The D_{it} was greatly reduced after FGA consistent with DFT calculations showing SiOx passivation of Ge.

Sulfur passivation of SiGe was found to prevent the GeO_x formation at the interface via Ge-S bond formation and assist Al-O-Si formation for direct bonding between $Al_2O_3/Si_{0.7}Ge_{0.3}$ [36]. It was observed that the sulfur passivated samples had lower Dit for high T Al_2O_3 ALD than HF(aq) passivated samples. Angle-resolved XPS of the Al_2O_3/SiGe interface showed the interlayer was mostly silicon suboxide. These data are consistent with the DFT calculations showing that a silicon suboxide interlayer during high-k growth on SiGe is favorable.

V. Conclusion.

The DFT-MD simulations were performed to investigate structural and electronic properties of a-HfO_2/a-SiO/SiGe with sub-oxide a-SiO interlayer *vs.* a-HfO_2/a-SiO_2/SiGe with fully-stoichiometric a-SiO_2 interlayer and a-HfO_2/a-SiO/Ge *vs.* a-HfO_2/a-SiO_2/Ge stacks. The coordination and electronic structure analysis demonstrates that the stacks with oxygen-deficient a-SiO interlayers form more ordered interfaces with fewer dangling bonds on semiconductor substrate than with a-SiO_2 interlayer. The stacks with fully-stoichiometric a-SiO_2 interlayer both for SiGe and Ge substrates create greater deformation in the semiconductor substrate upper layers leading to multiple dangling bonds and significant band-edge states decreasing stack bandgaps. The superior electric properties of oxygen-deficient a-SiO interlayer can be explained by the fact that under-coordinated Si atoms try to restore 4-fold coordination by forming bonds to the substrate semiconductor atoms creating almost a perfectly-ordered semiconductor interface. However, in case of fully-stoichiometric a-SiO_2 interlayers, Si prefers to form stronger Si-O bonds instead of Si-Ge creating Si-O-Ge bridges. This results in formation of highly irregular a-SiO_2/semiconductor interface with multiple dangling bonds and band-edge states significantly decreasing stack bandgaps both for SiGe and Ge substrates. To investigate effect of randomization, simulations were repeated for SiGe slab with randomized Si and Ge atoms. The SiGe(random) slab again demonstrates the superior electrical properties of a-SiO *vs.* a-SiO_2 interlayers. The stacks with SiGe(random) slab have slightly wider bandgaps than the stacks with SiGe(ordered) slab, since the randomized SiGe slab has only 50% of Ge atoms on upper slab surface instead of 100% Ge atoms on the upper surface of SiGe(ordered) slab.

The interface defects were passivated by H to investigate effect of passivation on electronic structure. After H passivation, most of the a-HfO_2/a-SiO_2/SiGe(ordered) and a-HfO_2/a-SiO_2/Ge defects were passivated significantly, expanding stack bandgaps.

Funding: The authors gratefully acknowledge support by TSMC and Applied Materials.

VI. References.

[1] D. Lu, P. Morin, B. Sahu, T. B Hook, P. Hashemi, A. Scholze, B. Kim, P. Kerber, A. Khakifirooz, P. Oldiges, K. Rim and B. Doris, Silicon Germanium FinFET Device Physics, Process Integration and Modeling Considerations, ECS Trans. 64 (2014) 337-345.

[2] T. Ando, P. Hashemi, J. Bruley, J. Rozen, Y. Ogawa, S. Koswatta, K. K. Chan, E. A. Cartier, R. Mo, and V. Narayanan, High Mobility High-Ge-Content SiGe PMOSFETs Using Al_2O_3/HfO_2 Stacks With In-Situ O_3 Treatment, IEEE Electron Dev. Lett. 38 (2017) 303-305.

[3] P. Hashemi, K. Balakrishnan, S. U. Engelmann, J. A. Ott, A. Khakifirooz, A. Baraskar, M. Hopstaken, J. S. Newbury, K. K. Chan, E. Leobandung, R. T. Mo and D.-G. Park, First demonstration of high-Ge-content strained-Si_{1-x} Ge_x ($x = 0.5$) on insulator PMOS FinFETs with high hole mobility and aggressively scaled fin dimensions and gate lengths for high-performance applications, IEDM Tech. Dig. (2014) 402-405.

[4] N. Miyata, H. Ishii, T. Itatani and T. Yasuda, Electron Mobility Degradation and Interface Dipole Formation in Direct-Contact HfO_2/Si Metal–Oxide–Semiconductor Field-Effect Transistors, Appl. Phys. Express 4 (2011) 101101-1 - 101101-3.

[5] P. J. Caplan, E. H. Poindexter, B. E. Deal, and R. R. Razouk, ESR centers, interface states, and oxide fixed charge in thermally oxidized silicon wafers, J. Appl. Phys. 50 (1979) 5847-5854.

[6] K. L. Brower and S. M. Myers, Chemical kinetics of hydrogen and (111) Si- SiO_2 interface defects, Appl. Phys. Lett. 57 (1990) 162-164.

[7] M. Hiratani, S. Saito, Y. Shimamoto, and K. Torii, Effective Electron Mobility Reduced by Remote Charge Scattering in High-κ Gate Stacks, Jpn. J. Appl. Phys. 41 Part 1 (2002) 4521-4522.

[8] M. Schmidt, M.C. Lemme, H. Kurz, T. Witters, T. Schram, K. Cherkaoui, A. Negara and P.K. Hurley, Impact of H_2/N_2 annealing on interface defect densities in Si(100)/SiO_2/HfO_2/TiN gate stacks, Microelectron. Eng. 80 (2005) 70-73.

[9] G. Kresse and J. Furthmuller, Efficiency of ab-initio total energy calculations for metals and semiconductors using a plane-wave basis set, Comput. Mater. Sci. 6 (1996) 15-50.

[10] G. Kresse and J. Furthmuller, Efficient iterative schemes for ab initio total-energy calculations using a plane-wave basis set, Phys. Rev. B 54 (1996) 11169-11186.

[11] P. Blöchl, Projector augmented-wave method, Phys. Rev. B 50 (1994) 17953-17979.

[12] G. Kresse and D. Joubert, From ultrasoft pseudopotentials to the projector augmented-wave method, Phys. Rev. B 59 (1999) 1758-1775.

[13] J. Perdew, K. Burke, and M. Ernzerhof, Generalized Gradient Approximation Made Simple, Phys. Rev. Lett. **77** (1996) 3865-3868.

[14] J. Perdew, K. Burke, and M. Ernzerhof, Generalized Gradient Approximation Made Simple [Phys. Rev. Lett. 77, 3865 (1996)], Phys. Rev. Lett. 78 (1997) 1396-1396.

[15] D. Ceresoli and D. Vanderbilt, Structural and dielectric properties of amorphous ZrO_2 and HfO_2, Phys. Rev. B 74 (2006) 125108-1-125108-6.

[16] H. Momida, T. Hamada, and Y. Takagi, Theoretical study on dielectric response of amorphous alumina, Phys. Rev. B 73 (2006) 054108-1-054108-10.

[17] X. Zhao, D. Ceresoli, and D. Vanderbilt, Structural, electronic, and dielectric properties of amorphous ZrO_2 from ab initio molecular dynamics, Phys. Rev. B 71 (2005) 085107-1-085107-10.

[18] D. Vanderbilt, X. Zhao, and D. Ceresoli, Structural and dielectric properties of crystalline and amorphous ZrO_2, Thin Solid Films 486 (2005) 125-128.

[19] V. Gritsenko, D. Gritsenko, S. Shaimeev, V. Aliev, K. Nasyrov, S. Erenburg, V. Tapilin, H. Wong, M. C. Poon, J. H. Lee, J. W. Lee, and C. W. Kim, Atomic and electronic structures of amorphous ZrO_2 and HfO_2 films, Microelectron. Eng. 81 (2005) 524-529.

[20] A. V. Shaposhnikov, D. V. Gritsenko, I. P. Petrenko, O. P. Pchelyakov, V. A. Gritsenko, S. B. Erenburg, N. V. Bausk, A.M. Badalyan, Yu. V. Shubin, T. P. Smirnova, H. Wong, and C. W. Kim, The atomic and electron structure of ZrO_2, J. Exp.

Theor. Phys. 102 (2006) 799-809.

[21] E. Chagarov, L. Porter, A. Kummel, Density-functional theory molecular dynamics simulations of a-HfO_2/Ge(100)(2×1) and a-ZrO_2/Ge(100)(2×1) interface passivation, J. Chem Phys. 144 (2016) 084704-1-084704-10.

[22] Y.-R. Luo, Bond Dissociation Energies in Diatomic Molecules, in CRC Handbook of Chemistry and Physics, W. M. Haynes, ed. 97th Edition (Internet Version 2017), CRC Press/Taylor & Francis, Boca Raton, FL, pp. 9-65-9-98.

[23] J. Heyd, G. E. Scuseria, and M. Ernzerhof, Erratum: "Hybrid functionals based on a screened Coulomb potential" [J. Chem. Phys. 118, 8207 (2003)], J. Chem. Phys. 124 (2006) 219906-219906.

[24] A. V. Krukau , O. A. Vydrov, A. F. Izmaylov, and G. E. Scuseria, Influence of the exchange screening parameter on the performance of screened hybrid functionals, J. Chem. Phys. 125 (2006) 224106-1-224106-5.

[25] W. Tang, E. Sanville, and G. Henkelman, A grid-based Bader analysis algorithm without lattice bias, J. Phys.: Condens. Matter 21 (2009) 084204-1-084204-7.

[26] M. Yu and D. R. Trinkle, Accurate and efficient algorithm for Bader charge integration, J. Chem. Phys. 134 (2011) 064111-1-064111-8.

[27] F. K. LeGoues R. Rosenberg, T. Nguyen, F. Himpsel, and B. S. Meyerson, Oxidation studies of SiGe, J. Appl. Phys. 65 (1989) 1724-1728.

[28] D. Nayak, K. Kamjoo, J. C. S. Woo, J. S. Park, and K. L. Wang, Rapid thermal oxidation of GeSi strained layers, Appl. Phys. Lett. 56 (1990) 66-68.

[29] D. K. Nayak, K. Kamjoo, J. S. Park, J. C. S. Woo, and K. L. Wang, Wet oxidation of GeSi strained layers by rapid thermal processing, Appl. Phys. Lett. 57 (1990) 369-371.

[30] H.K. Liou, P. Mei, U. Gennser, and E.S. Yang, Effects of Ge concentration on SiGe oxidation behavior, Appl. Phys. Lett. 59 (1991) 1200-1202.

[31] E. Chagarov, K. Sardashti, T. Kaufman-Osborn, S. Madisetti, S. Oktyabrsky, B. Sahu, and A. Kummel, Density-Functional Theory Molecular Dynamics Simulations and Experimental Characterization of a-Al_2O_3/SiGe Interfaces, ACS Appl. Mater. Interfaces 7 (2015) 26275-26283.

[32] T. Kaufman-Osborn, E. A. Chagarov, S. W. Park, B. Sahu, S. Siddiqui, A. C. Kummel, Atomic imaging and modeling of passivation, functionalization, and atomic

layer deposition nucleation of the SiGe(001) surface via H_2O_2(g) and trimethylaluminum dosing, Surf. Sci. 630 (2014) 273-279.

[33] T. J. Park, S. K. Kim, J. H. Kim, J. Park, M. Cho, S. W. Lee, S. H. Hong, and C. S. Hwang, Electrical properties of high-k HfO_2 films on $Si_{1-x}Ge_x$ substrates, Microelectron. Eng. 80 (2005) 222-225.

[34] M.-H. Cho, H. S. Chang, D. W. Moon, S. K. Kang, B. K. Min, D.-H. Ko, H. S. Kim P. C. McIntyre, J. H. Lee, J. H. Ku, and N. I. Lee, Interfacial characteristics of films grown on strained $Si_{0.7}Ge_{0.3}$ by atomic-layer deposition, Appl. Phys. Lett. 84 (2004) 1171-1173.

[35] B. De Jaeger, R. Bonzom, F. Leys, O. Richard, J. Van Steenbergen, G. Winderickx, E. Van Moorhem, G. Raskin, F. Letertre, T. Billon, M. Meuris and M. Heyns, Optimization of a thin epitaxial Si layer as Ge passivation layer to demonstrate deep sub-micron n- and p-FETs on Ge-On-Insulator substrates, Microelectron. Eng. 80 (2005) 26-29.

[36] K. Sardashti, K.-T. Hu, K. Tang, S. Park, H. Kim, S. Madisetti, P. McIntyre, S. Oktyabrsky, S. Siddiqui, B. Sahuf, N. Yoshida, J. Kachian, A. Kummel, Sulfur passivation for the formation of Si-terminated Al_2O_3/SiGe(001) interfaces, Appl. Surf. Sci. 366 (2016) 455-463.

Highlights

- **DFT MD simulations of a-HfO_2 on SiGe or Ge with a-SiO or a-SiO_2 interlayers.**
- **The electronic structure of the stacks was calculated with a HSE06 functional**
- **Stacks with a-SiO interlayer have superior electronic properties than with a-SiO_2**
- **After H passivation, most of the interface defects with a-SiO_2 layer are passivated**